Available online at www.sciencedirect.com
SCIENCE DIRECT®
Atmospheric Environment 39 (2005) 5343–5361
ATMOSPHERIC ENVIRONMENT
www.elsevier.com/locate/atmosenv

Spatial and temporal variability of PM levels and composition in a complex summer atmospheric scenario in Barcelona (NE Spain)

M. Viana[a,*], C. Pérez[b], X. Querol[a], A. Alastuey[a], S. Nickovic[c,1], J.M. Baldasano[b]

[a]*Institute of Earth Sciences "Jaume Almera", C/ Lluis Solé i Sabarís s/n, 08028 Barcelona, Spain*
[b]*Laboratory of Environmental Modelling, Universitat Politècnica de Catalunya (UPC), Avda. Diagonal 647 10.23, 08028 Barcelona, Spain*
[c]*Euro-Mediterranean Centre on Insular Coastal Dynamics (ICOD), University of Malta, Foundation for International Studies, Valleta, Malta*

Received 15 January 2005; accepted 23 May 2005

Abstract

Summer atmospheric coastal dynamics exert a significant influence on the levels and composition of atmospheric particulate matter (PM) in the North-Eastern Iberian Peninsula. Summer atmospheric scenarios in this region present a high degree of complexity as they are characterised by the absence of synoptic-scale air mass advections, the development of breeze circulations, enhanced photochemistry, local mineral dust re-suspension and the occurrence of African dust outbreaks. Three sampling sites were selected in Barcelona (NE Spain), an urban coastal site surrounded by complex topography. Regional dust modelling (DREAM) and high resolution meteorological modelling (MM5) were used to interpret PM levels and composition at the three sites. The results outline the effect of breeze dynamics and thermal internal boundary layer formation as the main meteorological drivers of the hourly evolution of PM levels. Levels of crustal components, secondary inorganic and carbon species are higher during the night, and only the marine aerosol content is higher during the day. Nitrate levels are higher during the night due to the thermal stability on NH_4NO_3. Sulphate levels are higher during the night as a consequence of the drainage flows. Lidar measurements and model results signalled the occurrence of two African dust episodes during the study period which mainly affected the free troposphere over Barcelona.

Keywords: PM10; PM2.5; PM1; Sea-land breeze; Western Mediterranean basin; Mesoscale modelling; African dust; Regional transport; Thermal internal boundary layer

1. Introduction

The current increasing interest in the study of atmospheric particulate matter (PM) is related to the identification of adverse effects on health (Dockery and Pope, 1996; Brunekreef et al., 1997; Künzli et al., 2000), climate and the environment (Arimoto, 2001;

*Corresponding author.
E-mail address: mviana@ija.csic.es (M. Viana).
[1]Actually at the World Meteorological Organisation (WMO), 7bis,avenue de la Paix, Case postale No. 2300 CH-1211 Geneva 2, Switzerland.

1352-2310/$ - see front matter © 2005 Elsevier Ltd. All rights reserved.
doi:10.1016/j.atmosenv.2005.05.039

IPCC, 2001). The levels and chemical composition of PM are determined not only by the emission sources, but also by atmospheric circulations which influence important factors such as dispersion, transport or stagnation of pollutants. In coastal areas, atmospheric dynamics have been studied by a number of authors. In Spain, Millán et al. (1991, 1997), Baldasano et al. (1994) and Gangoiti et al. (2001) have described the regional and long range transport processes of pollutants such as ozone along the Mediterranean coast. Toll and Baldasano (2000) and Soriano et al. (2001) have discussed the differences between the atmospheric circulation patterns in the Barcelona area under summer and winter conditions, as well as the singularities of summer atmospheric circulations in this area.

Levels and composition of PM10 and PM2.5, on the other hand, have been studied by Querol et al. (2001, 2003) and Querol et al. (2004) and Rodríguez et al. (2002) in Barcelona and the Western Mediterranean basin (WMB), respectively. The complexity of summer atmospheric scenarios as opposed to those of the winter months over the Iberian Peninsula (IP) is an important factor to be taken into account regarding the evaluation of PM levels. Winter pollution episodes are mainly dominated by stable anticyclonic conditions, which favour air mass stagnation and thus result in high PM, NO_X and organic matter and elemental carbon (OM + EC) levels. The summer months are characterised by the absence of large-scale forcing and the predominance of mesoscale circulations: the formation of a thermal low at a peninsular level forcing the convergence of surface winds from the coastal areas towards the central plateau with strong levels of subsidence over the WMB and sea-land breeze dynamics which result in the re-circulation and accumulation of pollutants over the eastern Iberian coast. Furthermore, due to the development of strong convective systems dust re-suspension strongly increases during the summer months. While minimum NO_x and OM + EC levels are registered during summer the same is not observed for PM levels (Querol et al., 2003). The NO_x summer minimum is not only related to the dilution in the increasing inland boundary layer depth but also to its destruction by photochemical reactions. Photochemical reactions are enhanced during summer months in contrast to winter. The higher temperatures and solar radiation result in the formation of secondary aerosols, contributing to the PM load. Sulphate levels also increase in summer due to the higher oxidation rate of SO_2 (Querol et al., 1999). Conversely, levels of particulate semi-volatile organic compounds (SVOCs) and nitrate decrease in summer as a consequence of their thermal instability.

In addition, external PM contributions such as African dust intrusions are more frequent during spring and summer (Rodríguez et al., 2001), and atmospheric scavenging is limited in summer due to the general absence of precipitation. Recently, Pérez et al. (2004) showed by means of lidar the presence of regional re-circulation aerosols at low levels and upper Saharan dust layers over Barcelona.

Consequently, summer atmospheric conditions at different scales exert a strong influence on various aspects of PM levels and composition. More specifically, the above studies performed in Eastern Spain have proved the significance of summer coastal circulation patterns on air quality. Thus, the present study aims to determine their influence on the levels and chemical composition of PM from diverse grain size fractions in the Barcelona area. To this end, a field campaign was devised during a 2-week period in the summer of 2001 (July 21–August 3) in which three sampling sites were selected for PM10, PM2.5 and PM1 monitoring. This campaign intended to measure PM levels in different environments within the city of Barcelona, and evaluate their daily variations under summer conditions (strong influence of breeze circulations). Two episodes of African air mass intrusion occurred during the study period.

2. Methodology

2.1. Measurements

PM levels at the three sites were continuously measured between July 21 and August 3 2001 by means of manual and automatic instrumentation. The three PM sampling sites are located on a transect from the coast (Olympic Harbour, 3) to the city (Sagrera, 1) to the range of Collserola (Fabra Observatory, 2), a NE–SW mountain range located to the NW of Barcelona (525 m.a.s.l., Fig. 1, bottom left). The instruments used for real time PM monitoring were GRIMM laser spectrometers, model 1107 at the Sagrera site and model 1108 at the Harbour and Fabra sites (for particle diameters $>0.25\,\mu m$). These instruments provided mean semi-hourly PM10, PM2.5 and PM1 levels. In parallel, manual PM samples were collected using high-volume gravimetric Andersen Graseby samplers for PM10 (reference instrumentation according to EN-12341) and high-volume MCV (Barcelona, Spain) samplers for PM2.5. Quartz fibre QF20 Schleicher and Schuell filters were used. The agreement between the automatic and manual instrumentation used in this study was observed and discussed by Querol et al. (2003). PM10 and PM2.5 sampling was carried out on a semi-daily basis (12 h; 06–18 and 18–06 UTC, 2 PM10 and 2 PM2.5 samples/day) from July 23 to 26, and on a daily basis (1 PM10 and 1 PM2.5 24 h samples/day) from July 30 to August 2. Bulk acid digestion and water extraction were applied to sub-samples, and chemical analyses included the determination of levels of major

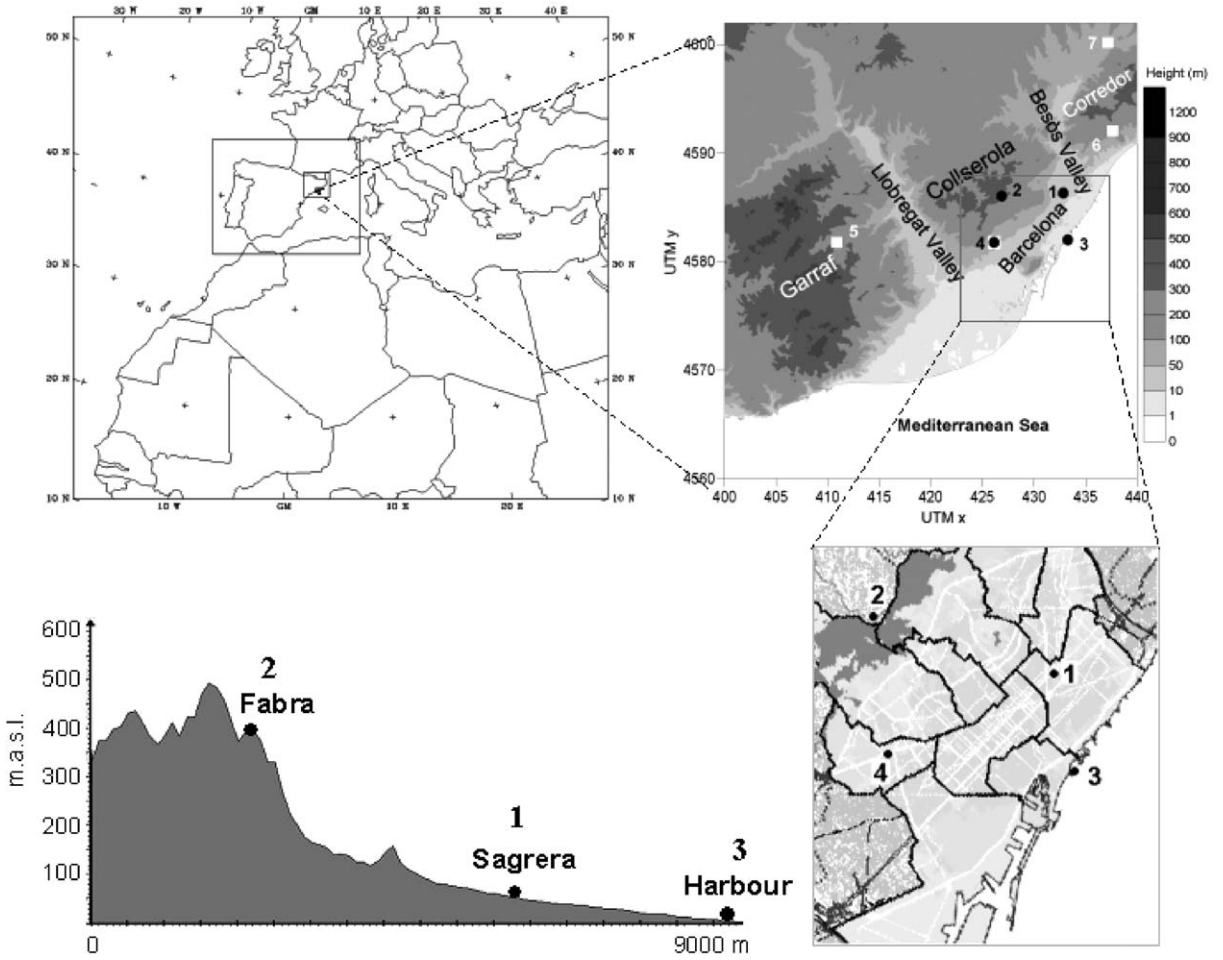

Fig. 1. (Top left) MM5 Four-nested domain configuration. (Top right) Location and orography of the Barcelona geographical area. Black circles indicate the location of the PM sampling sites (1, 2 and 3) and the lidar station (4). White squares indicate the location of the meteorological sites (lidar station,4; Vallirana, 5; Badalona, 6; Montmeló, 7) for model validation. (Bottom right) Location of the sampling sites over the city map: 1-Sagrera (sea level), 2-Fabra (400 m.a.s.l.), 3-Harbour (sea level), 4-lidar station. (Bottom left) Orography profile between 2 and 3.

and trace elements in the acidic solutions by ICP-AES and ICP-MS, of soluble anions (SO_4^{2-}, NO_3^-, Cl^-) in the water extracts by ion chromatography and of the total C content by a CHNS elemental analyser, as described by Querol et al. (2001). OM + EC levels were determined by applying a factor of 1.2 to the total C content. NH_4^+ analyses were performed by FIA colorimetry.

Additionally, the aerosol elastic-backscatter lidar system of the Technical University of Catalonia (UPC) (Fig. 1, bottom right, 4) based on a Nd:YAG laser emitting at 1064 nm (Rocadenbosch et al., 2000) performed diurnal cycle measurements during the study period (July 23, 26 and 30 and August 1) in order to help assessing the influence of African dust on PM levels and retrieve the height of the mixing layer. Lidar measurements at one wavelength can provide aerosol backscatter profiles using inversion techniques (Klett, 1981; Fernald, 1984). These techniques are generally subject to uncertainties because the lidar system equation contains two unknown parameters for one single equation $\alpha(\lambda)$ and $\beta(\lambda)$ which represent the aerosol extinction and backscatter coefficients. In order to solve the equation for the aerosol backscatter coefficient, a relationship between the two quantities, the so-called lidar ratio ($S(\lambda)$) has to be assumed. At Barcelona, the most powerful method that was found for single wavelength lidar signal inversion is a combination of the usual Klett (Klett, 1981) backward method applied with the comments from Fernald (1984) and Sasano and Nakane (1984) in an iterative process. In order to have an idea of

the concentrations in the dust plume, we first solved the equation for the aerosol backscatter coefficient assuming a lidar ratio of 60 sr. This value seems to be the most appropriate after African long range transport to western and northern Europe (Mattis et al., 2002; Müller et al., 2003; Ansmann et al., 2003). Secondly, we calculated from the aerosol model OPAC (Hess et al., 1998) a range of specific extinction cross section (σ^*_λ) for typical dust distributions which is the ratio of the extinction coefficient to the aerosol mass ($\sigma^*_{1064} = 0.5$ to $0.7\,m^2\,g^{-1}$)).

2.2. Models

In order to have a detailed picture of the synoptic and mesoscale processes during the episode a numerical simulation was run with the PSU/NCAR Mesoscale Model 5 (MM5), version 3, release 4 modelling system (Dudhia, 1993). Four nested domains (Fig. 1, top left) were selected which covered North Africa and Europe (Domain 1, D1), the IP (Domain 2, D2), the north-eastern IP (Domain 3, D3) and the Barcelona area (Domain 4, D4). D1 is formed by 135×150 grid points in the horizontal with 36-km grid-point spacing; D2, 97×124 12-km cells; D3, 64×64 4-km cells; and D4, 41×45 1-km cells. One-way nesting approach was used. The vertical resolution was of 29 σ-layers for all domains, the lowest one situated approximately at 10 m.a.g.l. and 19 of them below 1 km a.g.l. The upper boundary was fixed at 100 hPa. Initialisation and boundary conditions were introduced with final analysis data (FNL) of the National Weather Service's National Centers for Environmental Prediction (NCEP) Global Data Assimilation system (GDAS; Kanamitsu, 1989). The physics options used for the simulations were: MRF planetary boundary layer (PBL) as implemented in the NCEP MRF model (Hong and Pan, 1996), the Grell cumulus scheme (Grell et al., 1994), the Dudhia simple ice moisture scheme and the cloud-radiation scheme (MMMD/NCAR, 2001). In addition, the high-resolution domain was also simulated with the ETA PBL scheme (Janjic, 1994). Four meteorological stations located over the high-resolution domain were used to validate the model.

The Dust Regional Atmospheric Modeling (DREAM) system (Nickovic et al., 2001) was used to simulate the atmospheric cycle of African dust aerosol. It solves the Euler-type partial differential non-linear equation for dust mass continuity. DREAM is fully embedded as one of the governing equation in the atmospheric NCEP/Eta atmospheric model. The NCEP/Eta model provides in each time iteration step 3D values of atmospheric model parameters necessary for driving the dust concentration: horizontal and vertical velocities, temperature, humidity, turbulence mixing coefficients and soil surface parameters. The governing DREAM equation simulates all major processes of the atmospheric dust cycle. It describes dust production through simultaneous calculation of the input fluxes over dust sources, horizontal and vertical advection and turbulent mixing, and wet and dry dust deposition. In experiments shown in the article, dust mass is composed of the following four discrete particle size categories: clay (0.71 μm), small and large silt (6.1 μm, 18 mm), and sand (36 μm). For the synoptic-scale transport, only the first two dust classes are relevant for the analysis since their lifetime is larger than about 12 h.

3. The study area

The Barcelona region is dominated by four main features arranged parallel to the coastline: (1) the coastal plain, which comprises an 8-km strip of land between the sea and the first mountain range and which includes most of the cities in the greater urban area of Barcelona; (2) the coastal mountain range whose main peaks are Garraf (594 m), Collserola (512 m) and Corredor (657 m) (Fig. 1, top right); (3) the pre-coastal or Vallès depression, situated between the coastal mountain range and (4) the pre-coastal mountain range. There are two main river valleys perpendicular to the coast: Llobregat and Besòs which contain highways and roads that link Barcelona and its outlying towns with the cities in the Vallès depression. Many industries are located around these urban areas as well as in the above-mentioned valleys.

Two of the sampling sites (Sagrera and Harbour) were located in the city, while the Fabra Observatory site was located on the Collserola Range (Fig. 1, bottom left). The Harbour site was located on the terrace of a building at the sea front at the Barcelona Olympic Harbour, at about 15 m.a.s.l. The main local anthropogenic emissions in the area are related to harbour activities (vessel traffic), road traffic and industry. At the Sagrera site the instruments were placed in an air quality monitoring station belonging to the Departament de Medi Ambient of the Generalitat de Catalunya, which is located in a park at approximately 3 km from the coastline. Due to its location in a park this site could represent urban background conditions, but its proximity to the heaviest traffic avenue in Barcelona (Meridiana Avenue, located 150 m to the North) results in a strong traffic influence. Furthermore, the influence of industrial plants located along the Besòs and Llobregat rivers (NE and SW of Barcelona) may also be detected at this site. The Fabra site was located on the rooftop of the Fabra Astronomical Observatory in the Collserola forest, at approximately 400 m.a.s.l. Due to its high altitude and location, this site is not subject to the direct influence of the anthropogenic emissions

produced in the Barcelona city area, and it may be considered as a regional background site.

4. Meteorological scenario

4.1. Synoptic-scale patterns and African dust influence

The synoptic situation on July 20, 2001 was characterised by the sub-polar (Icelandic) low-pressure system to the north, the sub-tropical (Azores) high-pressure system pushing in over Europe and the WMB, a low-pressure system over Eastern Europe shifting east, and the North African and Iberian thermal lows.

During the whole study period, the sea level pressure situation remained rather constant with the typical summertime configuration (thermal low over the IP and anticyclonic circulation and subsidence over the WMB) (Figs. 2a–c). At higher levels, from July 21 a westerly wave formed with a N–S trough axis over the Atlantic ocean and a high-pressure enclosed circulation over North Africa (Fig. 2a) inducing south-western flows and the export of Saharan dust towards the IP. In the next days the high-pressure system at 700 hPa shifted west (not shown) and the northern edge of the Saharan dust plume reached the study area (see DREAM dust load map for July 24 at 12 UTC in Fig. 2d). Fig. 3a shows the range-corrected lidar signal at 1064 nm for July 23. African dust was observed in heights between 2 and 6 km in height. The structure of the plume is well-captured by DREAM (Fig. 3d). The lower boundary of the dust plume descended down to 1.5 km at 19 UTC. Lidar measurements were not performed on July 24. However, DREAM outlines the influence of African dust in the lowest atmospheric levels for that day (Fig. 3d). Between July 25 and 26 a weak westerly wave induced northern and western flows at 700 hPa over the study region developing into a low index circulation pattern from August 27 (Fig. 2b) which derived in the establishment of a deep cyclone centred southwest of Portugal and a high-pressure area over north Africa and the WMB on August 29 (Fig. 2c). DREAM (Fig. 2e) and the Seawifs maps (not shown) pointed out again the influence of the African dust plume between July 30 and August 3. The range-corrected lidar signal at 1064 nm for July 30 (Fig. 3b) and August 1 (Fig. 3c) clearly captured the penetration of Saharan dust into the boundary layer. The separation between Saharan dust in the free troposphere and aerosols in the boundary layer observed for July 23 had disappeared. Extinction profiles were derived from the Klett method assuming a lidar ratio of 60 sr. We coarsely estimate maximum concentrations in the dust plume at 2.3–2.4 km of $50\,\mu g\,m^{-3}$ for July 20 at 14 UTC and of $150\,\mu g\,m^{-3}$ for August 1 at 12 UTC assuming a specific extinction cross section of $0.6\,m^2\,g^{-1}$ for dust (Fig. 3d). Below 1.5–2 km African dust particles may be mixed with anthropogenic pollution. The general structure of the plume is fairly well-captured by DREAM (Fig. 3d) outlining the higher influence of African dust in the lowest levels from July 31 to August 3. DREAM delivers average surface concentrations of about $6\,\mu g\,m^{-3}$ in the period 23–25 July and $12\,\mu g\,m^{-3}$ in the period July 31–August 2 suggesting the higher influence of African dust on PM levels during the second episode (Fig. 4a).

4.2. Mesoscale patterns

Owing to its location at the sea front, the city of Barcelona is subject to the strong influence of breeze circulations during the summer months. The absence of large scale forcing (as pointed out in the previous section) and the development of mesoscalar flows related to the daily heating and cooling cycle (sea-land breezes, mountain-induced winds, valley winds and thermal lows) create regional re-circulations of pollutants over the eastern Iberian coast. On the local scale, solar radiation induces the development of sea breeze circulations during the day, and land breeze circulations during the night. The more usual pattern is characterised by the following processes: at break of day and until midday, the air masses traverse the coastal plain towards the Collserola Range, they ascend and are re-injected towards the sea in the coastal convective cell (Toll and Baldasano, 2000). The average mixing height (MH) in summer is low, oscillating between 400 and 800 m.a.s.l. in periods of maximum insolation at 5 km from the coastline over the lidar station. Usually after midday, the energy conveyed to the breeze by further solar heating allows it to traverse the Collserola Range (coastal), and even reach the pre-coastal range. The conjunction of the sea breeze and the anabatic winds produces air mass injections up to 2000–2500 m. Compensatory subsidence is induced in their return flow towards the sea. Pollution layers formed by injections at the coastal and pre-coastal mountain ranges at different times can be simultaneously detected between 800 and 1500 m over Barcelona (Pérez et al., 2004). At sundown, the progressive atmospheric cooling inverts the dynamics described above. As the boundary layer height decreases, the air masses descend from the coastal range and the river valleys towards the sea at a lower speed than that of the inland breeze.

5. PM levels

Mean daily PM10 levels for the study period at the three sites ranged from $31\,\mu g\,m^{-3}$ at Fabra to $45\,\mu g\,m^{-3}$ at the Harbour site and $57\,\mu g\,m^{-3}$ at Sagrera. Following the same behaviour, PM2.5 daily levels varied from $20\,\mu g\,m^{-3}$ at Fabra to $30\,\mu g\,m^{-3}$ at the Harbour site and

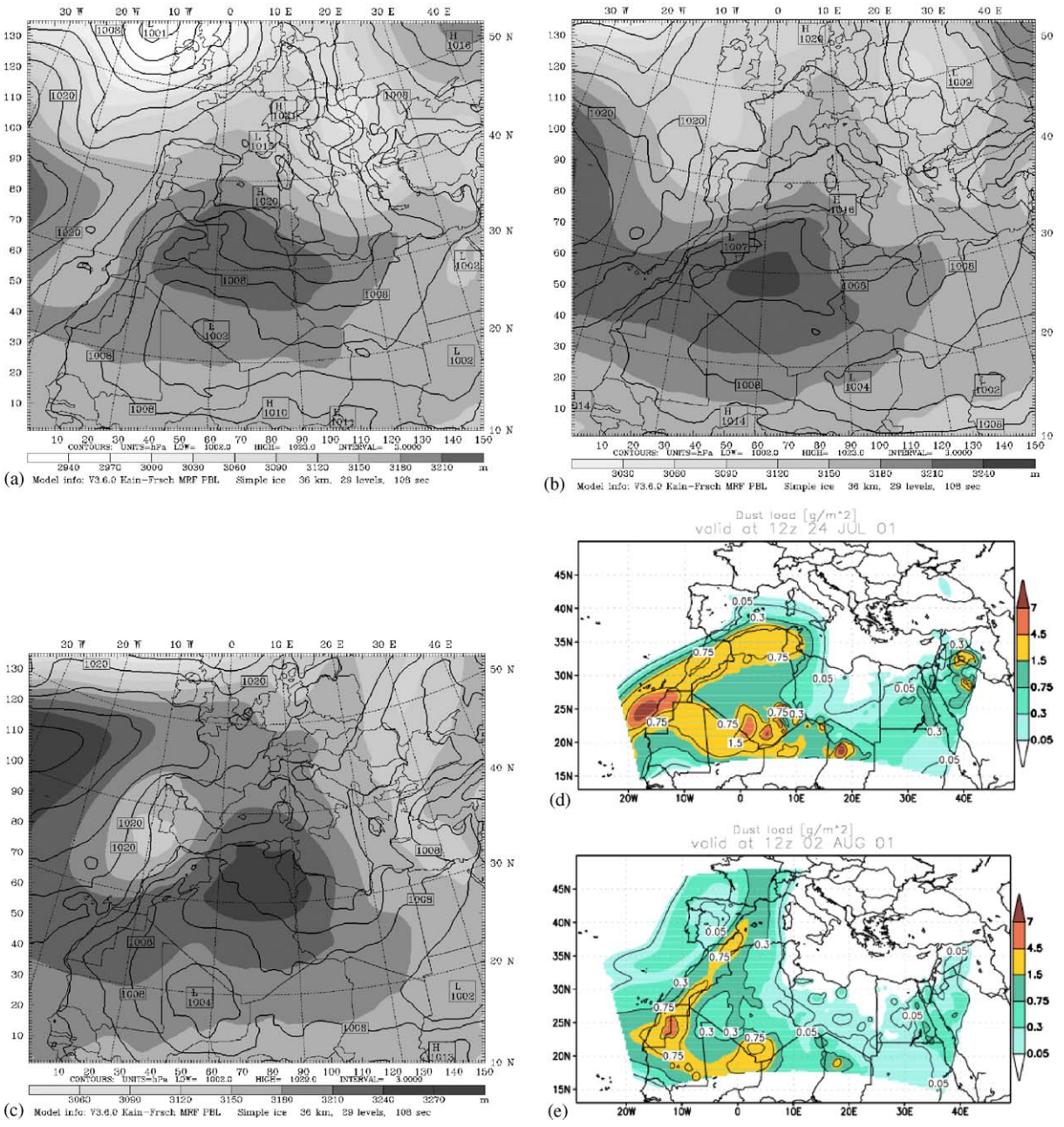

Fig. 2. Sea level pressure and Geopotential height at 700 Hpa at 12 UTC from Domain D1 for (a) July 21, (b) July 27, (c) July 29. DREAM dust load maps for (d) July 24 and (e) August 2.

35 $\mu g\,m^{-3}$ at Sagrera. Real time measurements of PM1 levels were lower at Fabra (7 $\mu g\,m^{-3}$) than at Harbour and Sagrera (17 and 18 $\mu g\,m^{-3}$, respectively). Thus, the daily averages show that the highest PM levels for all fractions were recorded at Sagrera, due to the high traffic influence. PM2.5/PM10 ratios were slightly lower at Sagrera than at Fabra and Harbour (0.6 at Sagrera vs. 0.7 at Fabra and Harbour), indicating that the particle size at the traffic site is larger than at the remaining sites due to coarse road dust re-suspension mainly derived from pavement abrasion and brake and tyre wear.

The daily evolution of mean PM levels throughout the study period at the three sites is shown in Figs. 4b–d. Sagrera and Harbour show similar PM10 trends. PM levels show a first increase from July 23 to 26–27, as a

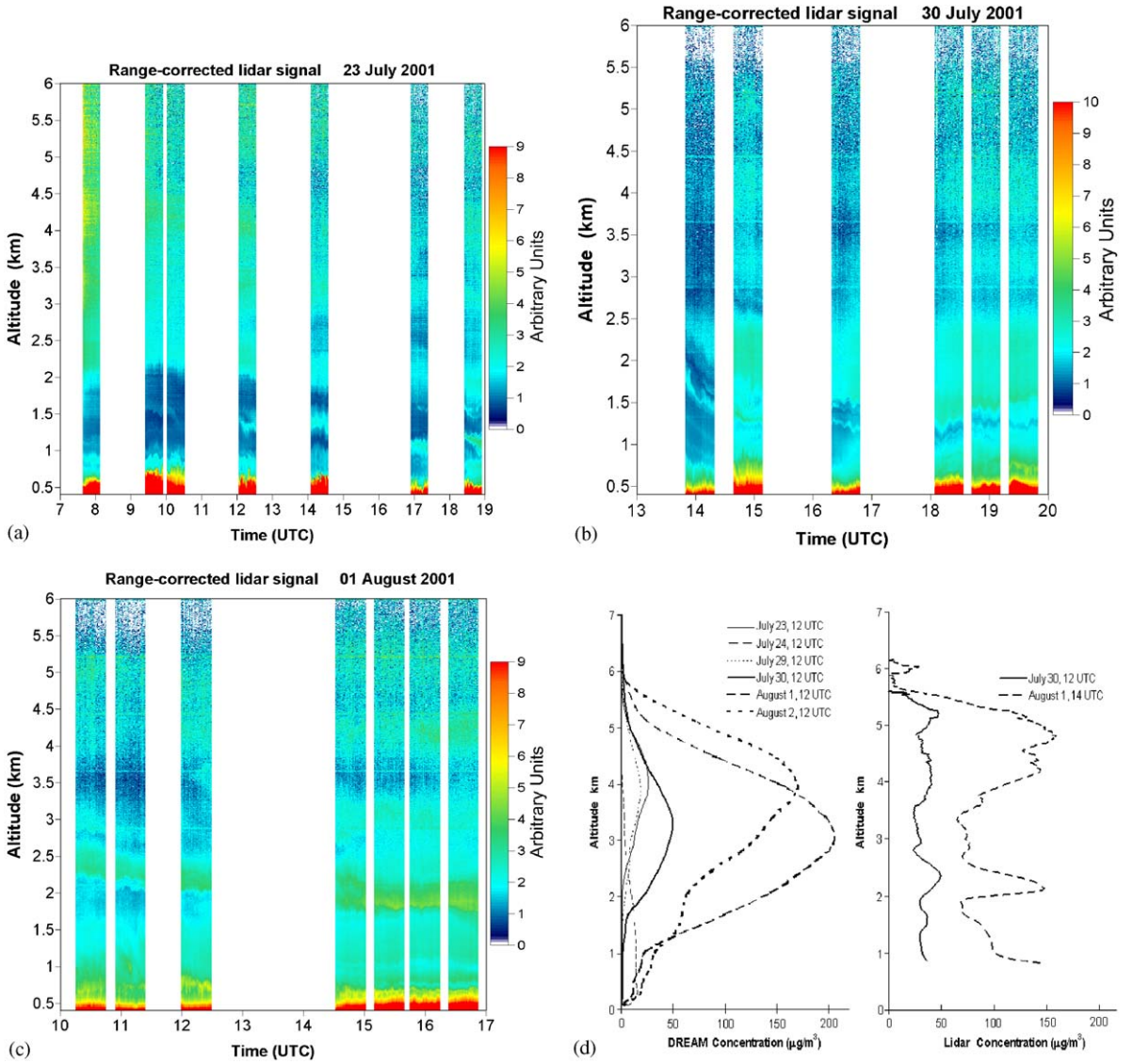

Fig. 3. (a–c) Range corrected 1064 nm signal (arbitrary units) (temporal resolution is 60 s) for July 23, July 30 and August 1. White columns indicate no measurements. Dark blue indicates weak backscattering and red indicates higher backscattering. (d-left) Vertical concentration profiles derived from DREAM. (d-right) Vertical concentration profiles derived from lidar assuming a lidar ratio of 60 sr and a specific extinction cross section of $0.6\,m^2\,g^{-1}$.

result of the direct traffic emissions and the regional re-circulation and accumulation of natural and anthropogenic pollutants caused by the stable, anticyclonic atmospheric scenario over the coast. As commented in Section 4.1, relatively low concentrations of African dust could be affecting PM levels during this period although its impact on the hourly evolution of PM levels is not detected (see next section). PM10 levels then show a slight decrease on 28–29 due to the weekend reduction of direct emissions over the city while PM2.5 and PM1 levels increase (also observed in Fabra) due to the fact that the finer fractions are strongly influenced by the formation and accumulation of secondary aerosols under this stagnant meteorological scenario. PM levels finally increase from the 30th once again as a consequence of working day emissions with local dust re-suspension coupled to the higher influence of the second African dust episode. Note that the grain size distribution at these two sites is dominated by the coarse fraction, due to the prevalence of mineral particles mainly from local (re-suspension) and in a minor amount from external (African) origin. The Fabra station, on the contrary, does not present the same daily evolution, owing to its location as a sub-urban site

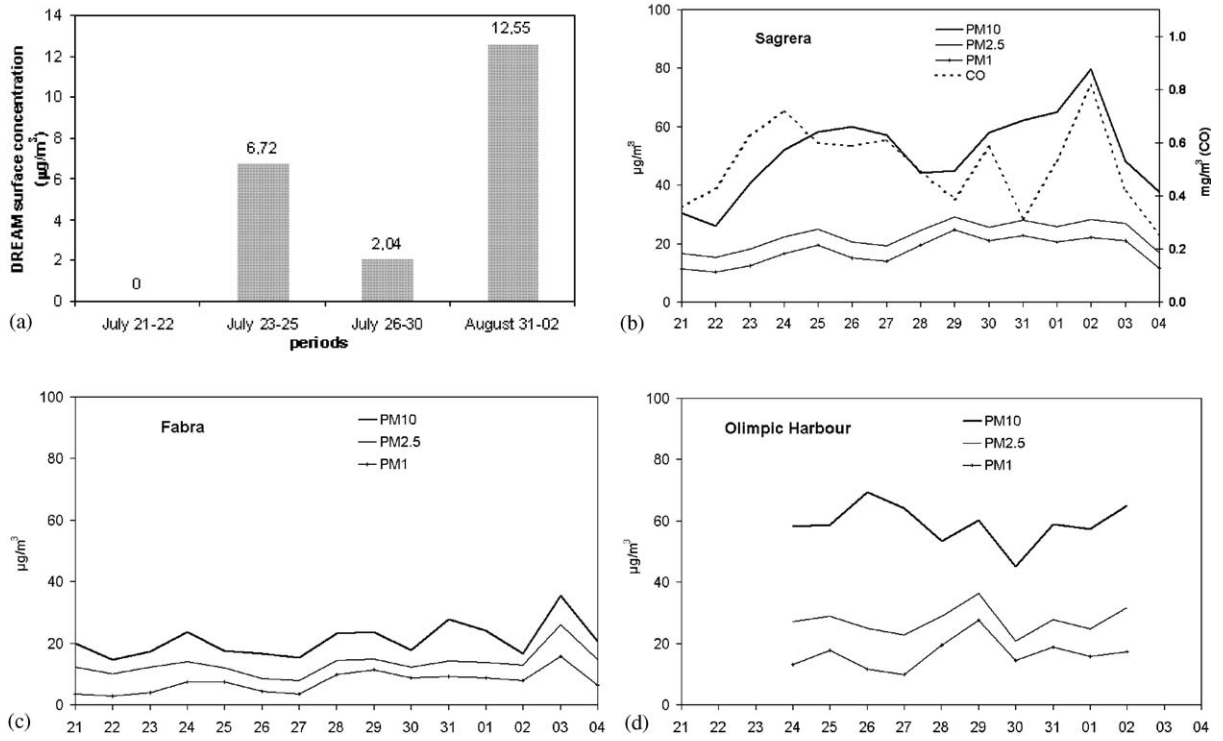

Fig. 4. (a) Average surface concentration derived from DREAM for 4 different periods. (b–d) Mean daily PM10, PM2.5 and PM1 levels recorded by laser spectrometry at the three sampling sites (Sagrera which also includes CO, Fabra, and Olympic Harbour).

at 400 m.a.s.l. on the Collserola Range. As will be exposed in the following sections, the main reasons for this are the absence of direct emissions at the site and the land breeze and catabatic winds system during the night.

5.1. Daily PM trends

In this section, a MM5 high-resolution simulation on July 26 is used to interpret the PM levels. The rest of the days showed similar patterns. Fig. 5a shows the MH evolution over the four sites derived from both MRF and ETA PBL schemes and the observed MH's by the lidar and the radiosounding at 12 UTC. Fig. 5b shows the comparison of surface wind speed and direction between model (MRF and ETA schemes) and observations at the lidar station and Fig. 5c summarises the bias and root mean square deviation (RMSD) of the model at the four meteorological stations displayed in Fig. 1. The MRF scheme clearly overestimates the MH while the ETA scheme agrees very well with the lidar and the radiosounding-derived MH's. Concerning wind speed and direction both schemes compare fairly well with observations and improve during the daytime. RMSD statistics of the ETA scheme show better general agreement with observations. Note that between 11 and 16 UTC the bias for wind speed outlines the tendency of the MRF scheme to underestimate surface winds. One of the known problems of the MRF scheme is that it tends to overestimate the ML growths and, hence, underestimates the surface winds. For example, Cheng et al. (2003) reported that the MM5 simulations with the MRF PBL scheme persistently overpredicted the PBL height over the Houston–Galveston area. Indeed, the surface wind vectors derived from the ETA scheme at different times during the day were used for interpretation of PM levels (Fig. 6). The most interesting feature of this comparison is that on both cases the diagnosed ML is deeper over the Fabra observatory and the lidar station than over Sagrera and the Olympic Harbour. Although mesoscale models do not include specific parameterisations for complex coastlines, the tendency exhibited by both schemes suggests the influence of a thermal internal boundary layer (TIBL) over the nearest stations to the coastline (Olympic Harbour and Sagrera). In summer, several phenomena interact at various scales driving the mixing layer (ML) evolution over Barcelona. Sea breeze flows generate a TIBL over the city as observed by Soriano et al. (2001). Sea breezes introduce cool and stable air over the coast. As the column of air advects downwind and warms, the temperature difference between the air and the ground lessens. As a result, the heat flux at the ground decreases, the ML warms less rapidly, and the rise rate of the MH is reduced (Stull, 1988). Generally, TIBLs do not extend

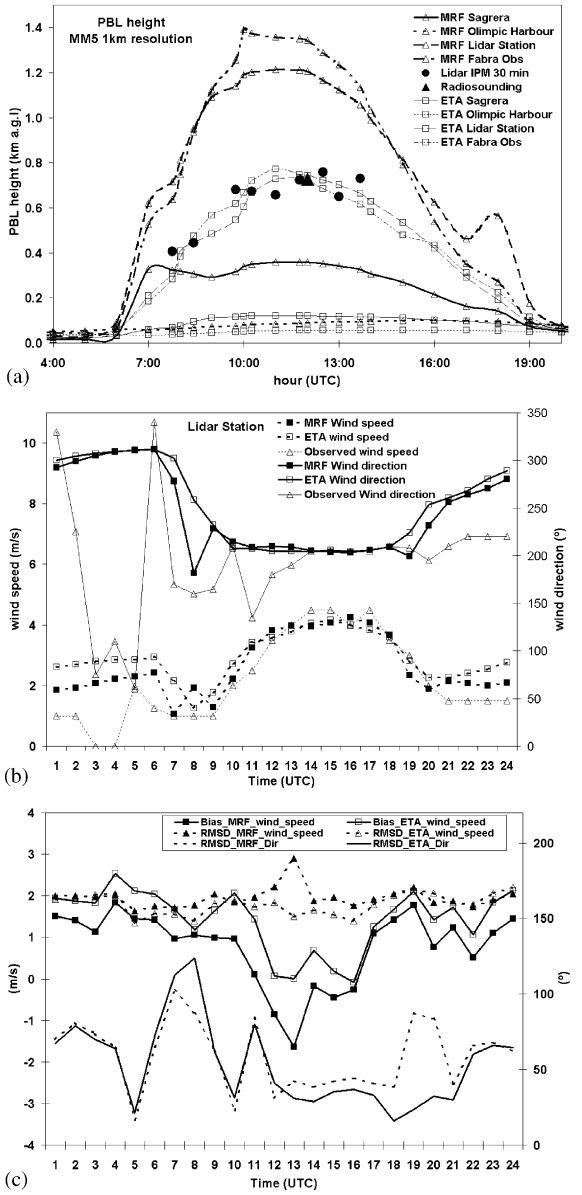

Fig. 5. (a) MM5 D4 Boundary layer evolution with MRF and ETA schemes on July 26 at the three sites and comparison with lidar and radiosounding-derived MH's. (b) Surface wind speed and direction at the lidar station from model (MRF and ETA schemes) and observations. (c) Bias and RMSD of the modelled wind speed and RMSD of the modelled wind direction.

all the way to the top of the marine air associated with the intruding air mass, so the remainder of the cool air mass above the TIBL and below the return flows, acts as well as a barrier for the TIBL vertical development. TIBLs deepen with distances downwind of the shoreline. These considerations will allow us to explain some of the characteristics of the PM levels registered over the three sites.

Fig. 7 shows the daily evolution of PM traffic emissions over the area on a working day of July from EMICAT2000 emissions inventory model (Parra, 2004) which includes emissions from road surface erosion (not particle dust re-suspension), brake and tyre wear, and exhaust. Although dust re-suspension could represent the major contribution it is also a useful information in order to better understand the daily PM behaviour.

5.1.1. Sagrera

The mean hourly evolution of PM10, PM2.5 and PM1 levels during the study period at the Sagrera site is shown in Fig. 8a and the hourly evolution on July 26 and August 1 is shown in Figs. 8b and c, respectively. Traffic is the main PM source at this site, as observed from the high degree of correlation between the hourly levels of PM10 and CO. PM levels at the Sagrera station register a maximum for all grain size fractions at 6–8 UTC (mean hourly maximum during the whole period of 90 μg PM10 m^{-3} and hourly maximum from 100 to 200 μg m^{-3} depending on the day). The strong morning peak at this site can be explained from the following considerations: emissions are high coinciding with the morning rush hour (Fig. 7), the MH is still small (Fig. 5a) and winds are weak (1 m s^{-1}) due to the morning sea breeze transition (Fig. 6a). The coarser particles (PM10) which present a more marked increase than the finer fractions (PM2.5/PM10 ratio = 0.3) outline the strong coarse dust re-suspension rates in the area. From 08 to 12 UTC levels decrease (mean hourly minimum of 40 μg PM10 m^{-3}) achieving a finer grain size distribution (PM2.5/PM10 ratio = 0.5) as on-road emissions are slightly reduced after the rush hour (thus decreasing coarser particle re-suspension), the ML grows and the sea breeze intensifies (3–4 m s^{-1}, S direction) diluting and advecting pollutants (Fig. 6b). This pollutant emission decrease was estimated by Parra and Baldasano (2004) in the form of a 0.4 t h^{-1} reduction in NO_x emissions in the Barcelona area. Although emissions increase from 13 to 16 UTC and remain high until 18–19 UTC, the sea breeze is fully active (4–6 m s^{-1}) until 16 UTC advecting pollutants inland (S–SE direction) (Fig. 6c). A new and progressive increase is detected after 18 UTC (40 μg PM10 m^{-3} at 18 UTC to 50 μg PM10 m^{-3} at 23 UTC), which lasts until 0–1 UTC the following day. This second increase is less pronounced than the morning rush hour one. A number of factors contribute to the afternoon–night pattern. Two relative maxima are observed (especially in the coarser fraction, PM2.5/PM10 ratio = 0.4). The influence from traffic emissions (although they are progressively reduced from 19 to 23 UTC) is coupled to the cooling of the atmosphere and large mesoscale compensatory subsidence, which result in the afternoon reduction of the MH and an increase in the concentration of pollutants. Transition to land breeze causing a

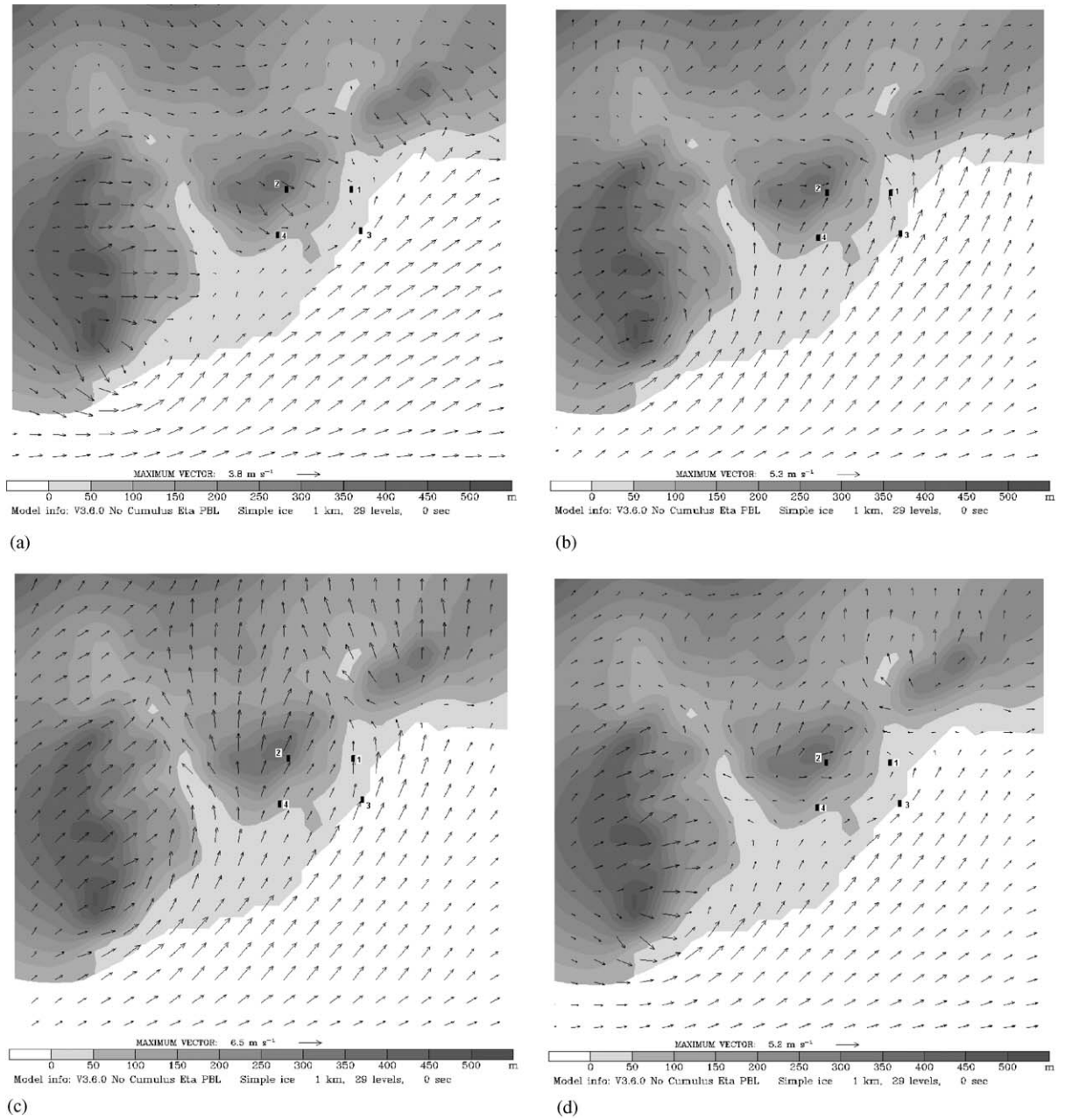

Fig. 6. Horizontal wind vectors and orography for July 26 over domain D4 (ETA scheme). (a) 06 UTC, (b) 09 UTC, (c) 16 (UTC), (d) 20 UTC. Black squares indicate the location of the sampling sites over the city.

reduction in wind speed (from 4–6 m s^{-1} during the day to 1–2 m s^{-1} during the night on July 26) and a change in wind direction (Fig. 5d) from S (the sea) to SW (the city) also contributes to this PM increase. In the particular case of July 26, although the evening transition is clearly captured by the model (compare Fig 6c and d), the large mesoscale anticyclonic circulation over the WMB which persists during the night (not shown) induces parallel flows to the shoreline. During some other days, the influence of the antyciclonic circulation was not so strong and NW or NE drainage flows over the city were dominant. Under both situations, the consequences are similar because the flows at night over Sagrera come from the city or the polluted adjacent valleys.

5.1.2. Fabra observatory

The mean hourly evolution of PM levels at the Fabra site is shown in Fig. 9a and the hourly evolution on July

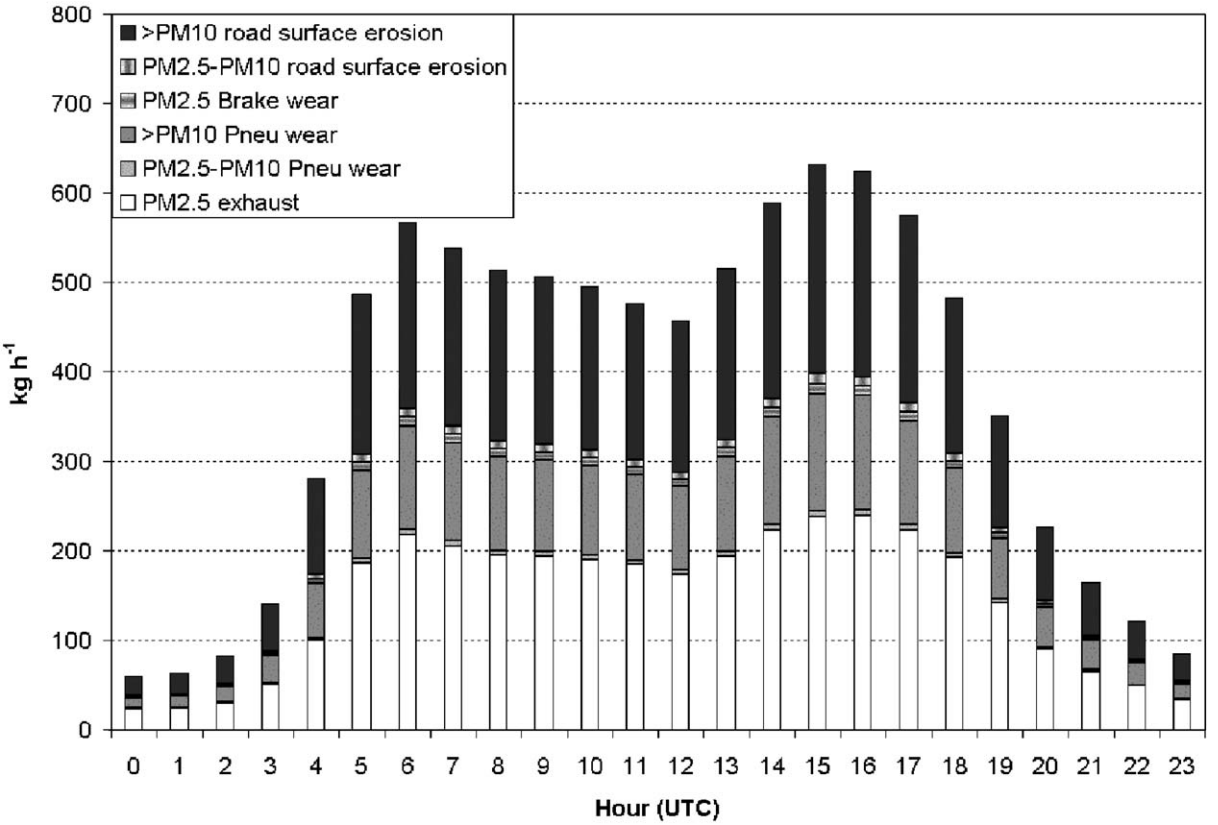

Fig. 7. Daily evolution of PM traffic emissions over the area on a working day of July from EMICAT2000 emissions inventory model (Parra, 2004).

26 and August 1 is shown in Figs. 9b and c, respectively. Owing to its location on the Collserola Range, this inland site does not receive the direct influence of anthropogenic emissions from the city of Barcelona. However, the hourly evolution presented in Fig. 8 is quite similar to the one described for Sagrera, indicating the existence of a link between the two sites. The transport of polluted air masses by the sea breeze and anabatic winds constitutes this link. Pollutants are emitted and accumulated in the urban area at around 5–8 UTC (mainly traffic related), and are subsequently transported inland by the sea breeze, ascending up the mountain side and reaching the study site (Fig. 6b). Consequently, the morning peak at Fabra is detected with a 1–2 h delay with respect to Sagrera (8–10 UTC, mean hourly maximum of 37 μg PM10 m^{-3} at 8 UTC, Fig. 9a). Despite the fact that the increase in PM10 is not as marked as in Sagrera due to the partial loss of coarse particles during transport, the prevalence of the coarse fraction and the decrease in the PM2.5/PM10 ratio is still marked (PM2.5/PM10 = 0.5 at 9 UTC).

As described for Sagrera, the increase of the MH and the reduction of on-road traffic results in the decrease in the PM levels at Fabra (hourly minimum of 13 μg PM10 m^{-3}) recorded from 10 UTC until approximately 14 UTC. Particle size distribution during this period is also finer (PM2.5/PM10 ratio = 0.8). A second and smoother increase is then detected from 14 to 19 UTC, a period in which the inland breeze is still active (Fig. 6c) and which reflects the transport of pollutants emitted (mainly by traffic) in the early evening in Barcelona. Finally, the MH decreases during the night and so do PM levels at Fabra (mean hourly minimum of 16 μg PM10 m^{-3} at 23 UTC). Minimum nighttime PM levels result from the absence of direct PM inputs and nighttime catabatic winds (Fig. 6d).

5.1.3. Harbour

The mean hourly evolution of PM levels at the Olympic Harbour is shown in Fig. 10a and the hourly evolution on July 26 and August 1 is shown in Figs. 10b and c, respectively. This station registers peak PM values up to 102 μg PM10 m^{-3} (mean hourly maximum at 6 UTC and hourly maximum from 150 to 250 μg m^{-3} depending on the day) between 22 and 7 UTC, and relatively low values during daytime (9–20 UTC, mean hourly minimum of 32 μg PM10 m^{-3} at 15 UTC). It is important to note that the minimum values registered at

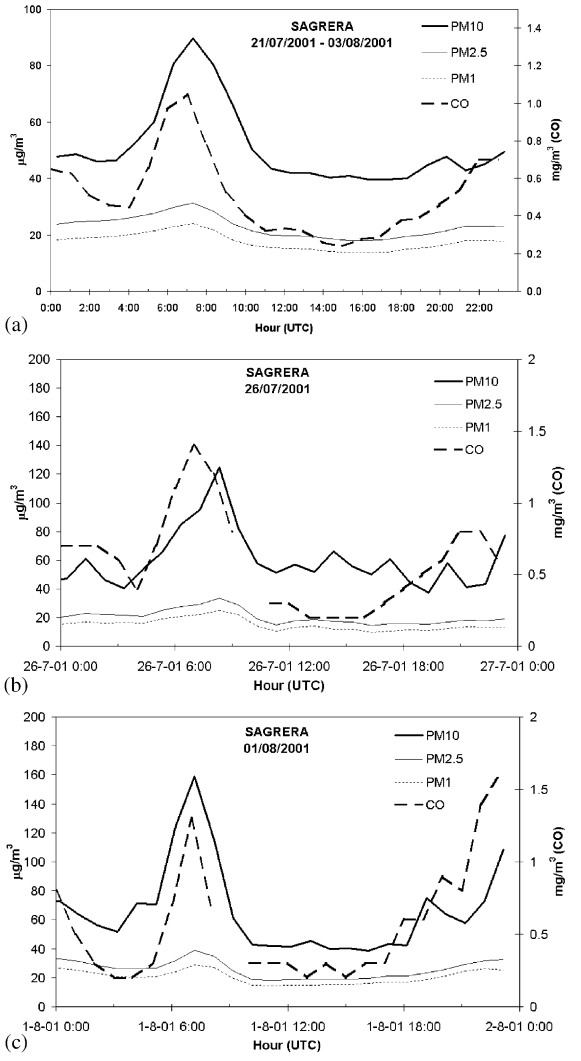

Fig. 8. (a) Mean hourly PM10, PM2.5, PM1 and CO levels at the Sagrera site from July 21 to August 4. (b) Hourly levels on July 26. (c) Hourly levels on August 1.

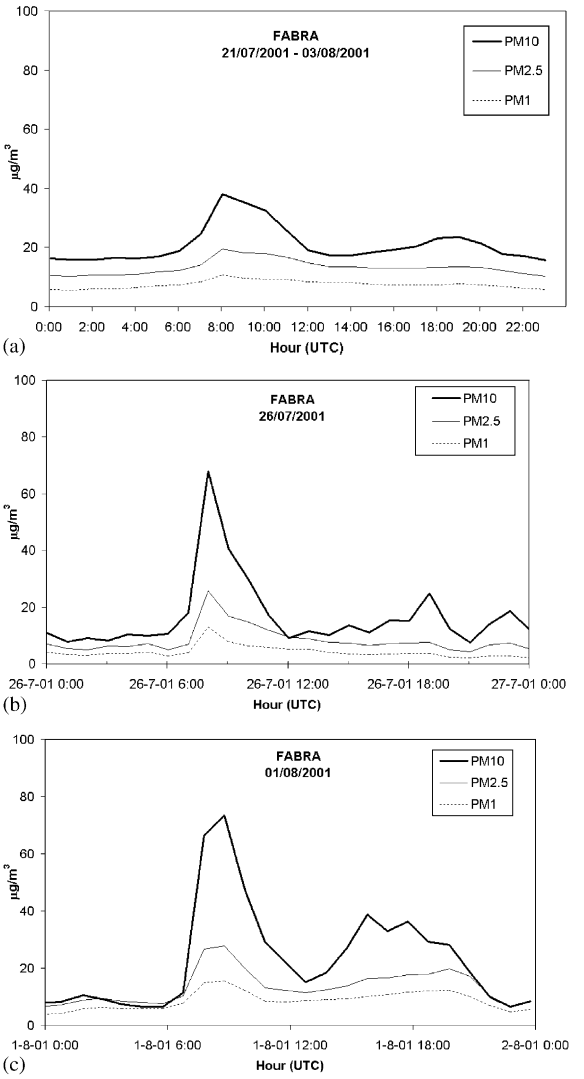

Fig. 9. (a) Mean hourly PM10, PM2.5 and PM1 levels at the Fabra site from July 21 to August 4. (b) Hourly levels on July 26. (c) Hourly levels on August 1.

this site are similar to the maximum levels registered at Fabra (32 µg PM10 m^{-3} at the Harbour vs. 37 µg PM10 m^{-3} at Fabra), thus highlighting the urban influence at the Harbour site. This site is located at the seafront and is clearly influenced by the land-sea transition. The effect of the atmospheric processes related to this transition on air quality over the area remains uncertain. As in the case of Sagrera, the morning peak between 6 and 8 UTC is related to traffic. We suggest that the higher values at this time over the Olympic Harbour could be due to the smaller height of the thermal internal boundary layer and the higher atmospheric stability of the atmosphere at this location together with weak winds (Fig. 6a). The deep decrease on PM levels from 8 to 16–18 UTC (mean hourly minimum of 31 µg m^{-3} at 15 UTC) is clearly related to the onset of the southern sea breeze introducing fresh air (Fig. 6b). The nigh time increase from 19 to 00 UTC follows similar reasons as Sagrera: PBL height reduction and change of wind direction and speed. The marked peak at around 3 UTC is related to nighttime summer harbour activities (mainly traffic), considering that its occurrence is relatively variable.

5.2. Daytime vs. nighttime PM levels

The sampling carried out between July 23 and 26 provided PM10 and PM2.5 samples corresponding approximately to day (from 06 to 18 UTC) and night

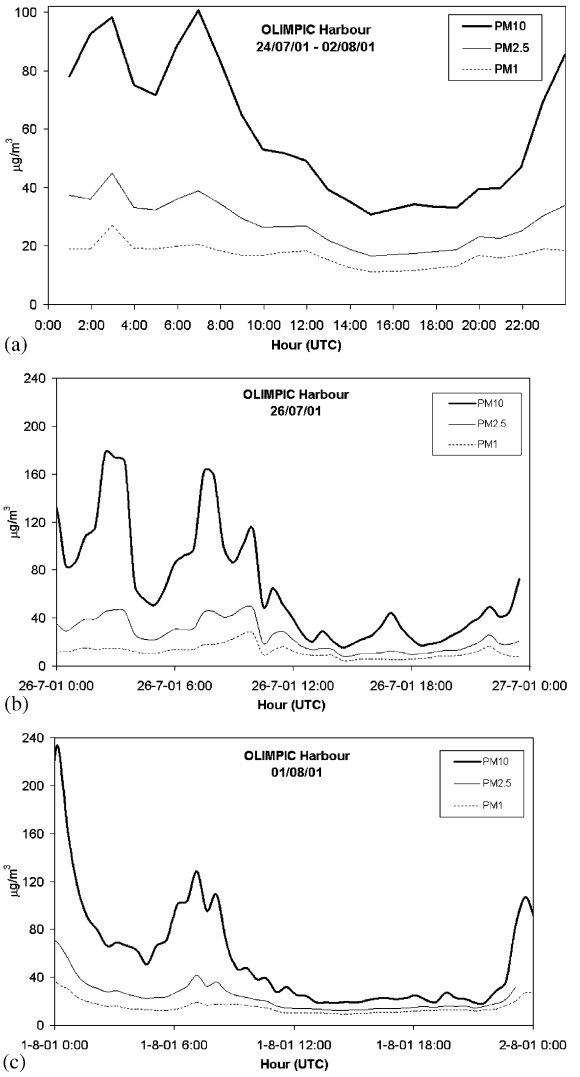

Fig. 10. (a) Mean hourly PM10, PM2.5 and PM1 levels at the Harbour site from July 24 to August 2. (b) Hourly levels on July 26. (c) Hourly levels on August 1.

(from 18 to 06 UTC) periods for the three sites. Fig. 11 shows the results obtained for PM10 (similar results obtained for PM2.5). The results register a daily oscillation of PM10 levels at all three sites, but two opposite trends are detected: one followed by the stations at sea level (Sagrera and Harbour) and another for the Fabra site (on the Collserola Range). At sea level, mean PM10 levels for July 23–26 are higher during the night (on average 59 $\mu g\,m^{-3}$ at Sagrera, 60 $\mu g\,m^{-3}$ at Harbour) than during the day (52 $\mu g\,m^{-3}$ at Sagrera, 42 $\mu g\,m^{-3}$ at Harbour). Conversely, at higher altitudes (Fabra), mean PM10 levels for July 23–26 are higher during the day (37 $\mu g\,m^{-3}$) and lower in the night

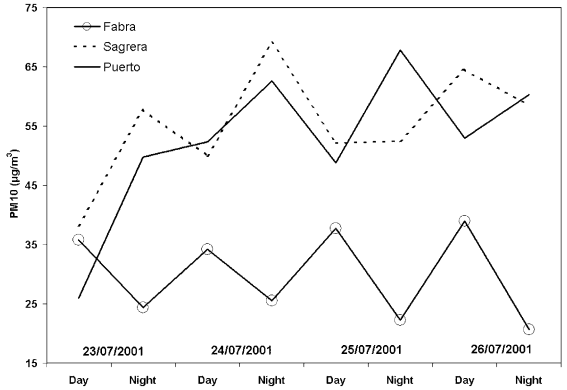

Fig. 11. Day–night oscillation of PM10 levels at Fabra, Sagrera and Harbour between July 23 and 26.

(23 $\mu g\,m^{-3}$). These opposite trends are a consequence of the atmospheric coastal dynamics described above.

6. Chemical composition

The results obtained from the chemical analysis of the PM10 and PM2.5 samples are presented below. Fig. 12 represents mean values for five components defined: organic matter and elemental carbon (OM + EC), secondary inorganic compounds (SIC: non-marine SO_4^{2-}, NH_4^+, NO_3^-), sea spray (Na, Cl^-, marine SO_4^{2-}), crustal components (CO_3^{2-}, SiO_2, Al_2O_3, Ca, K, Mg, Fe, P_2O_5) and the undetermined fraction (mostly water).

Fig. 12 shows the chemical composition of PM10 and PM2.5 at the three sites. In PM10, the OM + EC content ranges from 27–30% of the PM mass, although in terms of mass it increases from Fabra (8.4 $\mu g\,m^{-3}$) to Harbour (12.0 $\mu g\,m^{-3}$) to Sagrera (17.2 $\mu g\,m^{-3}$) with increasing traffic influence. Regarding SIC, the highest levels are registered at the Harbour and Sagrera sites (11.0 and 12.4 $\mu g\,m^{-3}$, respectively), whereas they reach 9.2 $\mu g\,m^{-3}$ at Fabra. However, the relative weight of SIC regarding the total PM10 mass is maximal at Fabra (30%) in contrast with 21–24% found at sea level. This relative increase towards higher altitudes reflects the longer atmospheric residence time of these compounds (fine grain size distribution). Coarser size particles (mainly mineral dust), on the other hand, sediment partially during transport. Levels of sea spray in PM10 are slightly higher at the Harbour (3%, 1.5 $\mu g\,m^{-3}$) and Sagrera (2%, 1.0 $\mu g\,m^{-3}$) sites given the proximity to the coast (Fabra, 2%, 0.6 $\mu g\,m^{-3}$). However, these levels of sea spray are very low when compared to the results obtained by Querol et al. (2003), where average ranges of 2–3 $\mu g\,m^{-3}$ of sea spray were found for coastal sites across the IP, and levels of 0.5–1.5 $\mu g\,m^{-3}$ at non-coastal sites. The high summer temperatures favour the

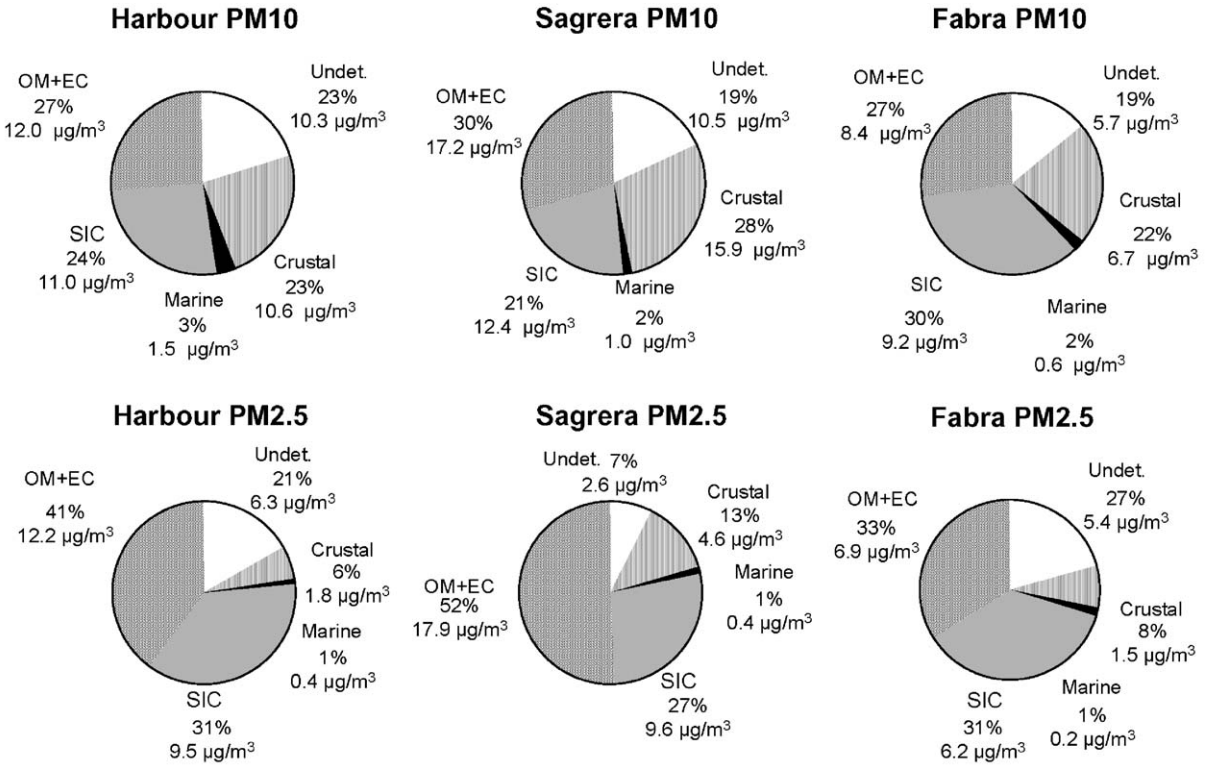

Fig. 12. Mean chemical composition of PM10 and PM2.5 at the three sites during the study period.

volatilisation of NH_4NO_3 and the formation of HNO_3, which in turn reacts with NaCl and results in the volatilisation of Cl as HCl, according to the reactions (Harrison and Pio, 1983; Warneck, 1988; Harrison and Kito, 1990; Wakamatsu et al., 1996; Pio and Lopes, 1998):

$$NH_4NO_3(s) \rightarrow HNO_3(s) + NH_3(g).$$

$$HNO_3(g) + NaCl(s) \rightarrow NaNO_3(s) + HCl(g).$$

Consequently, as $NaNO_3$ is formed and Cl is volatilised the levels of sea spray (Na + Cl + marine SO_4^{2-}) are much lower than expected according to the theoretical marine Cl/Na ratio of 1.16 eq eq^{-1} (Drever, 1982). Theoretical sea spray values for PM10 according to this ratio would be 2.0 μg m^{-3} at Sagrera, 2.8 μg m^{-3} at the Harbour and 1.3 μg m^{-3} at the Fabra site. These values would then coincide with the ranges described by Querol et al. (2003). Furthermore, as a consequence of these reactions the grain size distribution of NO_3^- tends to be coarse due to the reaction with Na, and significantly higher NO_3^- levels are found in PM10 than in PM2.5 at all sites (e.g. in Sagrera during daytime NO_3^- levels are 2.9 μg m^{-3} in PM10 and only 0.8 μg m^{-3} in PM2.5).

Finally, the average crustal load ranges between 22% and 28% of the PM10 mass, the maximum levels being recorded at Sagrera as a result of the re-suspension of road dust by traffic (in mass: Sagrera 15.9 μg m^{-3}, Harbour 10.6 μg m^{-3}, Fabra 6.7 μg m^{-3}). Crustal levels at Sagrera are thus more than two times higher than those found at Fabra, owing to the strong influence of road traffic at the first site. The largest differences between levels of PM components at sea level and the Fabra site are found in the crustal load, due to the coarser size of these particles and their segregation through transport.

The contribution of African dust to surface concentrations was relatively low during the study period when compared to other cases, due to the fact that these episodes were mainly confined to the upper atmospheric levels. The proportion of crustal components in PM10 at the three sites increased from the period July 23–25 (first African dust episode) to the period July 31–August 02 (second African dust episode) as shown in Fig. 13. This increase may be partly explained by the major amount of African dust during the last days of the study period which is consistent with lidar measurements (Fig. 3) and DREAM results (Fig. 4a).

Results obtained for PM2.5 show a similar pattern, as the highest OM + EC and crustal levels are recorded at Sagrera and the lowest at Fabra. The slightly higher OM + EC values registered in PM2.5 with respect to

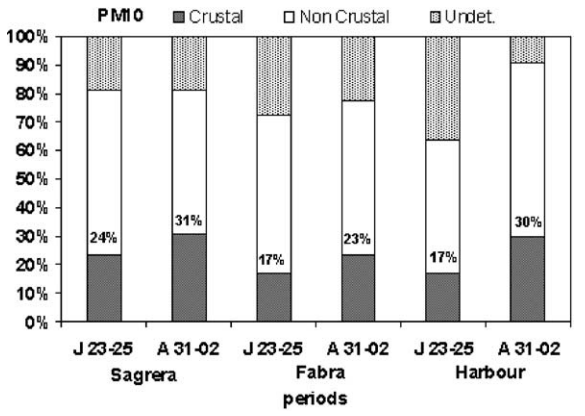

Fig. 13. Average crustal, non-crustal and undetermined fractions during the two African dust episodes for the three sites.

Table 1
Average concentration of trace elements in PM10 at the three selected sites

PM10	Fabra ($ng\,m^{-3}$)	Sagrera ($ng\,m^{-3}$)	Harbour ($ng\,m^{-3}$)
Li	0.4	0.9	0.8
Ti	28	66	51
V	8.9	18.2	19.8
Cr	3.8	10.1	6.2
Mn	10	25	19
Co	0.2	0.5	0.3
Ni	5.0	7.3	9.8
Cu	63	40	39
Zn	42	92	98
As	0.8	1.5	1.4
Sr	2.9	6.6	4.7
Cd	0.4	0.6	0.7
Ba	12	51	26
Pb	20	46	43

PM10 at Sagrera and Harbour are due to the fact that the sampling days do not coincide exactly due to technical problems with PM10 samplers. Levels of sea spray are reduced in PM2.5 owing to the coarse size of the particles. Levels of SIC are also higher at the Harbour and Sagrera than at Fabra. Finally, the crustal load at the three sites decreases with respect to PM10. It is interesting to note that there is only a small difference between the crustal load measured in PM2.5 at Fabra and Harbour (city shore and sub-urban site, 1.8 and $1.5\,\mu g\,m^{-3}$, respectively) with respect to the higher load detected at the traffic site of Sagrera ($4.6\,\mu g\,m^{-3}$). This difference is caused by the significant contribution of road dust to the PM2.5 fraction, despite the fact that this contribution usually predominates in the coarser sized fraction. This was not as evident in PM10, where larger differences were observed.

A number of trace elements were also analysed for PM10 and PM2.5. Table 1 shows the results obtained for PM10. The sum of the trace elements analysed adds up to $0.4\,\mu g\,m^{-3}$ at Sagrera whereas it represents $0.3\,\mu g\,m^{-3}$ at Harbour and $0.2\,\mu g\,m^{-3}$ at Fabra. These elements constitute $<1\%$ of the PM10 mass at all sites. The levels of the majority of the elements are higher at Sagrera (Li, Ti, Cr, Mn, Co, As, Sr, Ba, Pb), as a reflection of the direct influence of anthropogenic emissions. At the Harbour site, however, levels of V, Ni, Zn and Cd are highest, probably because of the influence of two power plants located along the coast. The only element which registers higher levels at Fabra is Cu, although the possible source is still unidentified.

6.1. Daytime vs. nighttime chemical composition

The mean chemical composition of the daytime and nighttime samples collected for all three sites is summarised in Tables 2 and 3. In PM10 (Table 2), at sea level three out of the four PM components defined (crustal, SIC and OM + EC) increase during the night as a consequence of the land–sea transport, whereas the only component to increase during the day is the sea spray (owing to the sea breeze contribution). This behaviour is common to the Sagrera and Harbour sites. Conversely, at Fabra levels of all four components are higher during daytime.

The day–night variations of the crustal fraction are different for the three study sites. In Sagrera the relative weight of the crustal fraction does not vary significantly between day and night, as it represents 27% and 26% of the PM10 mass, respectively. The high crustal daytime levels measured at Sagrera ($13.9\,\mu g\,m^{-3}$) contrast with those obtained at Fabra and the Harbour (7.4, $6.3\,\mu g\,m^{-3}$), and indicate that they result from the high traffic influence at this site. The high nighttime levels at Sagrera ($15.2\,\mu g\,m^{-3}$) are similar to those registered at the Harbour ($13.9\,\mu g\,m^{-3}$), and thus may be attributed to the drainage flows. At the Fabra site the crustal components reach higher levels during the day ($7.4\,\mu g\,m^{-3}$) than during the night ($4.0\,\mu g\,m^{-3}$), due to the diurnal breeze flow that transport urban air masses towards this site.

When compared with PM2.5 (Table 3), the results show that levels of PM2.5 components present smaller day–night variations, and that these mainly concern the finer PM components (SIC and OM + EC). At sea level, significant day–night variations are detected for SIC and OM + EC at Sagrera and Harbour. The levels of these components are again higher during the night. As recorded for PM10, at Fabra OM + EC and SIC crustal component levels are higher during the day. However,

Table 2
Mean chemical composition of the major PM10 components analysed in the daytime and night time samples collected at the three sites between July 23 and 26

	Sagrera		Fabra		Harbour	
	Day	Night	Day	Night	Day	Night
PM10	52	59	37	23	42	60
OM + EC	16.2	19.1	11.8	6.3	9.7	13.7
$CO_3^=$	3.5	3.5	1.7	0.8	1.2	2.9
SiO_2	4.7	5.4	2.7	1.6	2.5	5.4
Al_2O_3	1.6	1.8	0.9	0.5	0.8	1.8
Ca	2.4	2.3	1.2	0.5	0.8	2.0
K	0.4	0.5	0.2	0.1	0.2	0.5
Na	0.8	0.7	0.6	0.4	1.1	0.9
Mg	0.3	0.3	0.2	0.1	0.2	0.3
Fe	1.0	1.3	0.5	0.2	0.4	1.0
P_2O_5	0.1	0.1	0.1	0.0	0.1	0.1
SO_4^{2-}anthrop	5.7	6.2	5.3	4.8	5.6	6.1
SO_4^{2-}marine	0.2	0.2	0.2	0.1	0.3	0.2
NO_3^-	2.9	4.3	1.7	0.7	2.0	3.1
Cl	0.2	0.3	0.1	<0.1	0.1	0.2
NH_4^+	1.6	1.9	1.1	1.1	1.0	1.1
Undetermined	10.2	11.7	9.7	5.5	16.2	21.0
Crustal	13.9	15.2	7.4	4.0	6.3	13.9
Marine	1.2	1.1	0.8	0.6	1.5	1.4
SIC	10.2	12.4	8.1	6.6	8.6	10.3
OM + EC	16.2	19.1	11.8	6.3	9.7	13.7

OM + EC: organic matter and elemental carbon; SIC: secondary inorganic compounds ($SO_4^{2-} + NO_3^- + NH_4^+$).

Table 3
Mean chemical composition of the major PM2.5 components analysed in the daytime and night time samples collected at the three sites between July 23 and 26

	Sagrera		Fabra		Harbour	
	Day	Night	Day	Night	Day	Night
PM2.5	30	36	27	20	27	34
OM + EC	16.4	19.8	10.6	6.1	10.5	15.2
$CO_3^=$	0.7	0.5	0.2	0.2	0.3	0.3
SiO_2	0.9	0.7	0.7	0.6	0.9	0.7
Al_2O_3	0.3	0.2	0.2	0.2	0.3	0.2
Ca	0.5	0.3	0.2	0.1	0.2	0.2
K	0.2	0.2	0.1	0.1	0.1	0.1
Na	0.2	0.3	0.2	0.2	0.3	0.2
Mg	0.1	0.1	0.0	0.0	0.0	0.0
Fe	0.3	0.3	0.1	0.1	0.1	0.2
P_2O_5	0.1	0.1	0.0	0.0	0.0	0.0
SO_4^{2-}anthrop	5.2	5.7	4.5	4.4	6.0	6.1
SO_4^{2-}marine	0.1	0.1	0.1	0.0	0.1	0.1
NO_3^-	0.8	1.6	0.4	0.2	0.4	1.0
Cl	<0.1	0.1	<0.1	<0.1	<0.1	0.1
NH_4^+	1.7	2.0	1.3	1.1	1.3	1.1
Undetermined	2.8	4.1	8.2	7.0	5.7	8.9
Crustal	3.1	2.4	1.5	1.2	1.9	1.8
Marine	0.3	0.4	0.3	0.3	0.4	0.4
SIC	7.7	9.3	6.1	5.7	7.7	8.2
OM + EC	16.4	19.8	10.6	6.1	10.5	15.2

OM + EC: organic matter and elemental carbon; SIC: secondary inorganic compounds ($SO_4^{2-} + NO_3^- + NH_4^+$).

the low proportion of the marine component (coarse size) in PM2.5 does not present significant variations throughout the day as it is mainly found in PM10.

Certain of the PM elements and compounds analysed, such as Cl^-, Na, SO_4^{2-}, NO_3^- or NH_4^+ also present interesting day–night variations. Na, for example, presents higher daytime levels at all sites as expected from the marine breeze circulations, which are however not observed for Cl^- (Table 2). Levels of Cl^- are relatively constant throughout the day and lower than the theoretical equivalent to marine Na, as explained above, resulting from the volatilisation of this element due to the higher daytime availability of HNO_3.

Furthermore, excess of $NO_3^- + SO_4^{2-}$ in the ionic balance with NH_4^+ indicates a significant deficit of NH_4^+, which probably results from the reaction with Cl^- and its subsequent volatilisation. Due to the thermal stability of NH_4NO_3, NH_4^+ levels are higher at nighttime.

The thermal stability of NH_4NO_3 also results in higher nighttime NO_3^- levels observed at sea level (Table 2). This trend coincides with the results obtained at a larger scale by Querol et al. (2003), who detected a constant winter increase of NO_3^- levels throughout the Spanish territory. The winter conditions when compared to the summer may be considered equivalent to nighttime conditions on a daily basis. The same study also detected a common SO_4^{2-} summer maximum resulting from the higher oxidation rate of SO_2. Consequently, higher SO_4^{2-} levels were expected to be obtained at daytime for this study. However, the results proved that SO_4^{2-} also increases during the night as a consequence of the transport towards the sea of polluted air masses transported inland during the day by the sea breeze.

7. Conclusions

PM10, PM2.5 and PM1 levels were sampled and monitored between July 21 and August 3 in the Barcelona (Spain) mountainous-coastal area under a complex summer atmospheric scenario, characterised by the absence of synoptic-scale air mass advections, the development of breeze circulations, enhanced photochemistry, local mineral dust re-suspension and African

dust contributions. The following conclusions may be extracted from the results:

- PM transport and dispersion during the summer months in the study area are dominated by the sea breeze dynamics and TIBL formation. Breeze circulations and transitions (enhanced sea breeze during the day and weak land breeze during the night) are reflected in the hourly PM levels at the three selected sites in the form of consecutive maxima. The levels and hourly variations of PM at the three sites are mainly regulated by traffic emissions together with sea breeze regime and TIBL structure.
- High morning PM levels at the Harbour could be related to atmospheric stability over the shoreline and breeze direction and speed while the deep afternoon decrease is related to the onset of the southern sea breeze introducing fresh air. PM levels increase during the night at sea level (Sagrera and Harbour) and during the day on the Collserola Range (Fabra). This outlines the effect of the land breeze dynamics at sea level (accumulation of pollutants during the night). In the case of the Fabra site, nighttime PM levels are lower as a result of the absence of PM inputs from the city by means of land breeze and catabatic winds.
- The chemical composition of PM10 is a function of the major local emission sources at the different sites. Levels of crustal components and OM + EC are higher at Sagrera (16 and 17 $\mu g\,m^{-3}$, respectively) due to the traffic influence. Levels of sea spray are higher at the Harbour site (1.5 $\mu g\,m^{-3}$). SIC levels are slightly higher at the urban and traffic sites (Sagrera, 12; Harbour, 11 $\mu g\,m^{-3}$) than at the sub-urban site (Fabra, 9 $\mu g\,m^{-3}$), although the relative weight (%) of SIC at Fabra is higher than at sea level as a consequence of the sedimentation of coarser particles through transport.
- Cl^- levels are lower than expected (according to the theoretical marine ratio of 1.16 $eq\,eq^{-1}$ and to levels obtained by other authors in the same study area) due to volatilisation as HCl, favoured by the presence of HNO_3 resulting from the thermal instability of NH_4NO_3. As a consequence of these reactions the grain size distribution of NO_3^- increases, and it is mainly found in the coarse fraction in the form of $NaNO_3$.
- The crustal contribution to PM2.5 is reduced with respect to PM10. However, at the Sagrera traffic site (4.6 $\mu g\,m^{-3}$) the crustal levels are more than two times higher than those at the Harbour and Fabra sites (1.8 and 1.5 $\mu g\,m^{-3}$), thus reflecting that the crustal fraction in PM2.5 is highly influenced by traffic.
- The comparison of day and night samples (12 h) reveals that, at sea level, levels of crustal components, SIC and OM + EC are higher during the night than during the day. The marine aerosol content is higher during the day. In PM2.5 the nighttime increase is especially evident for the finer components (SIC and OM + EC).
- NO_3^- levels in PM10 at sea level are higher during the night, due to the thermal stability on NH_4NO_3. Contrarily to what was expected, SO_4^{2-} levels are also higher during the night, as a consequence of the night drainage flows.
- Two African dust episodes were detected during the study period which mainly affected the free troposphere. The quantitative influence of African dust on the chemical composition of PM10 cannot be assessed as it is mixed with local dust. The occurrence of these episodes did not alter the hourly evolution of PM levels at any of the sites. Levels of crustal components increased from the first to the second episode. Lidar measurements and the DREAM dust model suggest that this could be partly explained by the major influence of the second episode on the levels of crustal components.

Acknowledgements

The authors would like to thank the Spanish Ministry of the Environment and the Departament de Medi Ambient of the Generalitat de Catalunya for supporting this study and the CICYT project REN2003-09753-C02. They are also indebted to the Fabra Astronomical Observatory and the Barcelona Olympic Harbour for providing the locations where the instruments were set, and to the UPC lidar Group for providing complementary lidar measurements of the episode. The FNL meteorological database and satellite images provided by NASA/Goddard Space Flight Center, NOAA-ARL and the SeaWIFS-NASA Project, respectively, are highly appreciated.

References

Ansmann, A., Bösenberg, J., Chaikovsky, A., Comerón, A., Eckhardt, S., Eixmann, R., Freudenthaler, V., Ginoux, P., Komguem, L., Linné, H., López Márquez, M.A., Matthias, V., Mattis, I., Mitev, V., Müller, D., Music, S., Nickovic, S., Pelon, J., Sauvage, L., Sobolewsky, P., Srivastava, M.K., Stohl, A., Torres, O., Vaughan, G., Wandinger, U., Wiegner, M., 2003. Long-range transport of Saharan dust to northern Europe: the 11–16 October 2001 outbreak observed with EARLINET. Journal of Geophysical Research 108 (D24), 4783.

Arimoto, R., 2001. Eolian dust and climate: relationships to sources, tropospheric chemistry, transport and deposition. Earth-Science Reviews 54, 29–42.

Baldasano, J.M., Cremades, L., Soriano, C., 1994. Circulation of air pollutants over the Barcelona geographical area in summer. Proceedings of Sixth European Symposium Physico-Chemical Behaviour of Atmospheric Pollutants. Varese (Italy), 18–22 October, 1993. Report EUR 15609/1: 474-479.

Cheng, F., Byun, D., Kim, S., 2003. Sensitivity study of the effects of land surface characteristics on meteorological simulations during the TexAQS2000 period in the Houston-Galveston area. 13th PSU/NCAR Mesoscale Model Users' Workshop, June 10–11, Boulder, CO.

Brunekreef, B., Janssen, N.A.H., Harssema, H., Knape, M., Vliet, P.V., 1997. Air Pollution from truck traffic and lung function in children living near motorways. Epidemiology 8, 8.

Dockery, D., Pope, A., 1996. Epidemiology of acute health effects: summary of time-series studied. In: Spengler, J.D., Wilson, R. (Eds.), Particles in Our Air: Concentration and Health Effects. Harvard University Press, pp. 123–147.

Drever, J.J., 1982. The Geochemistry of Natural Waters. Prentice-Hall Inc, Englewood Cliffs, NJ 437pp.

Dudhia, J., 1993. A non-hydrostatic version of the penn State-NCAR mesoscale model: validation tests and simulation of an Atlantic CYCLONE and cold front. Monthly Weather Review 121, 1493–1513.

Fernald, F.G., 1984. Analysis of atmospheric lidar observations: some comments. Applied Optics 23, 652–653.

Gangoiti, G., Millán, M.M., Salvador, R., Mantilla, E., 2001. Long-range transport and re-circulation of pollutants in the western mediterranean during the project regional cycles of air pollution in the west-central mediterranean area. Atmospheric Environment 35, 6267–6276.

Grell, G.A., Dudhia, J., Stauffer, D.R., 1994. A description of the fifth-generation Penn State/NCAR mesoscale model (MM5). NCAR Technical Note, NCAR/TN-398 + STR, 117 pp.

Harrison, R.M., Kito, A.M.N., 1990. Field intercomparison of filter pack and denuder sampling methods for reactive gaseous and particulate pollutants. Atmospheric Environment 24, 2633–2640.

Harrison, R.M., Pio, C., 1983. Size differentiated composition of inorganic aerosol of both marine and continental polluted origin. Atmospheric Environment 17, 1733–1738.

Hess, M., Koepke, P., Schult, I., 1998. Optical properties of aerosols and clouds: The software package OPAC. Bulletin of the American Meterolological Soceity 79, 831–844.

Hong, S.-Y., Pan, H.-L., 1996. Nonlocal boundary layer vertical diffusion in a medium-range forecast model. Monthly Weather Review 124, 2322–2339.

IPCC, 2001. Climate Change 2001: The Scientific Basis. IPCC. Cambridge University Press, Cambridge.

Janjic, Z.I., 1994. The step-mountain eta coordinate model: further development of the convection, viscous sublayer, and turbulent closure schemes. Monthly Weather Review 122, 927–945.

Kanamitsu, M., 1989. Description of the NMC global data assimilation and forecast system. Weather and Forecasting 4, 335–342.

Klett, J.D., 1981. Stable Analytical inversion solution for processing lidar returns. Applied Optics 20, 211–220.

Künzli, N., Kaier, R., Medina, S., Studnicka, M., Chanel, O., Filliger, P., Herry Jr., M.F.H., Puybonnieux-Texier, V., Quénel, P., Schneider, J., Seethaler, R., Vergnaud, J.C., Sommer, H., 2000. Public health impact of outdoor and traffic related air pollution: a European assessment. The Lancet 356, 795–801.

Mattis, I., Ansmann, A., Müller, D., Wandinger, U., Althausen, D., 2002. Dualwavelength Raman lidar observations of the extinction-to-backscatter ratio of Saharan dust. Geophysical Research Letters 29 (9), 1306.

Millán, M.M., Artíñano, B., Alonso, L., Navazo, M., Castro, M., 1991. The effect of meso scale flows and long range atmospheric transport in the western Mediterranean area. Atmospheric Environment 25 (5/6), 949–963.

Millán, M., Salvador, R., Mantilla, E., Kallos, G., 1997. Photooxidant dynamics in the Mediterranean basin in summer: results from European research projects. Journal of Geophysical Research 102, 8811–8823.

MMMD/NCAR, 2001. PSU/NCAR Mesoscale Modeling System Tutorial Class Notes and User's Guide: MM5 Modeling System Version 3.

Müller, D., Mattis, I., Wandinger, U., Althausen, D., Ansmann, A., Dubovik, O., Eckhardt, S., Stohl, A., 2003. Saharan dust over a central European EARLINET-AERONET site: Combined observations with Raman lidar and Sun photometer. Journal of Geophysical Research 108 (D12), 4345.

Nickovic, S., Kallos, G., Papadopoulos, A., Kakaliagou, O., 2001. A model for prediction of desert dust cycle in the atmosphere. Journal of Geophysical Research 106, 18113–18129.

Parra, R., 2004. Development of the EMICAT2000 model for the estimation of air pollutants emissions from Catalonia and its use in photochemical dispersion modelling. Ph.D. Thesis. Technical University of Catalonia, http://www.tdx.cesca.es/TDX-0803104-102139/ (in Spanish).

Parra, R., Baldasano, J.M., 2004. Modelling the on-road traffic emissions from Catalonia (Spain) for photochemical air pollution research. Weekday—weekend differences. Proceedings of the Air Pollution 2004, 30/6-2/7/2004, Rhodes.

Pérez, C., Sicard, M., Jorba, O., Comerón, A., Baldasano, J.M., 2004. Summertime re-circulations of air pollutants over the north-eastern Iberian coast observed from systematic EARLINET lidar measurements in Barcelona. Atmospheric Environment 38 (24), 3983–4000.

Pio, C.A., Lopes, D.A., 1998. Chlorine loss from marine aerosol in a coastal atmosphere. Journal of Geophysical Research 103, 25263–25272.

Querol, X., Alastuey, A., Lopez-Soler, A., Plana, F., Mantilla, E., Juan, R., Ruiz, C.R., Orden, A.L., 1999. Characterisation of atmospheric particulates around a coal-fired power station. International Journal of Coal Geology 40 (2–3), 175–188.

Querol, X., Alastuey, A., Rodríguez, S., Plana, F., Ruiz, C.R., Cots, N., Massagué, G., Puig, O., 2001. PM10 and PM2.5 source apportionment in the Barcelona Metropolitan Area, Catalonia, Spain. Atmospheric Environment 35 (36), 6407–6419.

Querol, X., Alastuey, A., Rodríguez, S., Viana, M.M., Artíñano, B., Salvador, P., Mantilla, E., Santos, S.G.D., Patier, R.F., Rosa, J.D.L., Campa, A.S.D.L., Menedez, M., 2003. Estudio y evaluación de la contaminación atmosférica por material particulado en España: Informes finales. IJA-

CSIC, ISCIII, CIEMAT, Universidad de Huelva, Universidad del País Vasco.

Querol, X., Alastuey, A., et al., 2004. Levels of particulate matter in rural, urban and industrial sites in Spain. The Science of Total Environment 334–335, 359–376.

Rocadenbosch, F., Soriano, C., Comerón, A., Baldasano, J.M., Rodríguez, A., Muñoz, C., García-Vizcaíno, D., 2000. 3D scanning portable backscatter lidar platform for atmospheric remote sensing: performance and architecture overview V. In: Russell, J.E., Schäfer, K., Lado-Bordowsky, O. (Eds.), Remote Sensing of Clouds and the Atmosphere. Proc. SPIE 4168, pp. 158–169.

Rodríguez, S., Querol, X., Alastuey, A., Kallos, G., Kakaliagou, O., 2001. Saharan dust contributions to PM10 and TSP levels in Southern and Eastern Spain. Atmospheric Environment 35, 2433–2447.

Rodríguez, S., Querol, X., Alastuey, A., Plana, F., 2002. Sources and processes affecting levels and composition of atmospheric aerosol in the Western Mediterranean. Journal of Geophysical Research 107 (D24), 4777.

Sasano, Y., Nakane, H., 1984. Significance of the extinction/backscatter ratio and the boundary value term in the solution for the two-component lidar equation. Applied Optics 23, 11–12.

Soriano, C., Baldasano, J.M., Buttler, W.T., Moore, K.M., 2001. Circulatory patterns of air pollutants within the Barcelona air basin in a summertime situation: lidar and numerical approaches. Boundary-Layer Meteorology 98, 33–55.

Stull, R.B., 1988. An Introduction to Boundary Layer Meteorology. Kluwer Academic Publishers, Dordreeht 670pp.

Toll, I., Baldasano, J.M., 2000. Modeling of photochemical air pollution in the Barcelona area with highly disaggregated anthropogenic and biogenic emissions. Atmospheric Environment 34, 3069–3084.

Wakamatsu, S., Utsunomiya, A., Han, J.S., Mori, A., Uno, I., Uehara, K., 1996. Seasonal variation in atmospheric aerosol concentration covering Northern Kyushu, Japan and Seoul, Korea. Atmospheric Environment 30, 2343–2354.

Warneck, P., 1988. Chemistry of the natural atmosphere. International Geophysics Series, vol. 41. Wiley, New York, Academy Press, London, 757pp.